# Measurement of Electron Density Fluctuations Using O-Mode Microwave Imaging Reflectometry in a TST-2 Spherical Tokamak*)

Yoshio NAGAYAMA, Akira EJIRI[1)], Yuichi TAKASE[1)], Naoto TSUJII[1)], Hideya NAKANISHI[2)], Masaki OHSUNA[2)], Hayato TSUCHIYA[2)] and Soichiro YAMAGUCHI[3)]

*College of Science and Technology, Nihon University, 1-8-14 Kanda Surugadai, Chiyoda-ku, Tokyo 101-8308, Japan*
[1)]*Graduate School of Frontier Sciences, The University of Tokyo, 5-1-5 Kashiwanoha, Kashiwa 277-8561, Japan*
[2)]*National Institute for Fusion Science, 322-6 Oroshi-cho, Toki 509-5292, Japan*
[3)]*Faculty of Engineering Science, Kansai University, 3-3-35 Yamate-cho, Suita 564-8680, Japan*

(Received 30 November 2019 / Accepted 27 May 2020)

An O-mode microwave imaging reflectometry system has been installed in a spherical tokamak named TST-2. The illumination wave frequency is 23 - 32 GHz, which corresponds to the cutoff electron density of 0.65 - $1.3 \times 10^{19}$ m$^{-3}$. The microwave image of the scattered wave is formed on an imaging detector named horn-antenna millimeter-wave imaging detector by imaging optics that consist of an ellipsoidal aluminum mirror, a Teflon lens, and a dielectric plate. The detected channel numbers are 6 (poloidal) × 6 (toroidal) × 2 (radial). The data of power and phase of the scattered wave are sampled every 0.5 μs and are stored by the LABCOM system at the National Institute for Fusion Science via a private network named SNET. The scattered wave quickly fluctuates (~5 μs) and has a large amplitude (>100 times). From the time evolution of the phase at the internal reconnection event, it is inferred that the reduction in amplitude may be owing to the phase mixing of scattered wave in each detector channel.



Keywords: microwave, imaging, reflectometry, plasma, ST, TST-2, electron density, fluctuation, IRE

DOI: 10.1585/pfr.15.2402060

## 1. Introduction

Spherical tokamak (ST) is a novel confinement concept that is suitable for a fusion reactor [1]. Because the plasma current in ST is much higher than that in a tokamak of the same size, instabilities in STs may differ from those in tokamaks. For example, internal reconnection events (IREs) are often observed in STs [2]. IRE is similar to the disruption in tokamaks because IRE causes an abrupt reduction in the thermal energy in ST, which is similar to the disruption in a tokamak. However, there are some different features. In tokamaks, the disruption destroys flux surfaces in a radially wide region and often leads to plasma termination. In ST, IRE destroys flux surfaces in a radially localized region.

Because instabilities induce electron density fluctuations, visualization of 2D or 3D electron density fluctuations will be useful for investigating instabilities in fusion plasmas. Plasma reflects the ordinary mode (O-mode) microwave at the cutoff frequency ($\omega_{pe}/2\pi$), i.e.,

$$\frac{\omega_{pe}}{2\pi}[\mathrm{GHz}] = 28.4\sqrt{n_e\,[10^{19}\mathrm{m}^{-3}]}. \quad (1)$$

An O-mode microwave imaging reflectometry (MIR) instrument is a device for producing a microwave image of the cutoff layer that may represent density fluctuation [3].

MIR has been intensively developed at the National Institute for Fusion Science (NIFS) for the TPE-RX RFP device [3, 4] and for the large helical device (LHD) [5–8]. In the last MIR experiment at LHD [8], a newly developed horn-antenna millimeter-wave imaging detector (HMID) [9, 10] was employed. This paper describes the O-mode MIR system (O-MIR), which is installed in the Tokyo Spherical Tokamak 2 (TST-2) [11], and preliminary results on the electron density fluctuation measurements on IRE in TST-2 are presented.

## 2. O-MIR System in TST-2

The schematic diagram of the O-MIR system in TST-2 is shown in Fig. 1. This system consists of the MIR optics in TPE-RX [5] and the O-MIR electronics in LHD [8]. The multi-frequency microwave is illuminated by the MIR optics, which forms a plasma image on HMID. The electronics consist of an radio frequency (RF) circuit, HMID, frequency separator, and detectors. The RF circuit generates microwave and reference waves for phase detection. HMID detects a microwave image of plasma. The output of HMID is the intermediate frequency (IF) wave. Frequency separator separates microwaves, which reflect at different layers. The output of frequency separator is the second IF (IF2) wave, which has the same frequency of

*author's e-mail: nagayama.yoshio@nihon-u.ac.jp*
*) This article is based on the presentation at the 28th International Toki Conference on Plasma and Fusion Research (ITC28).

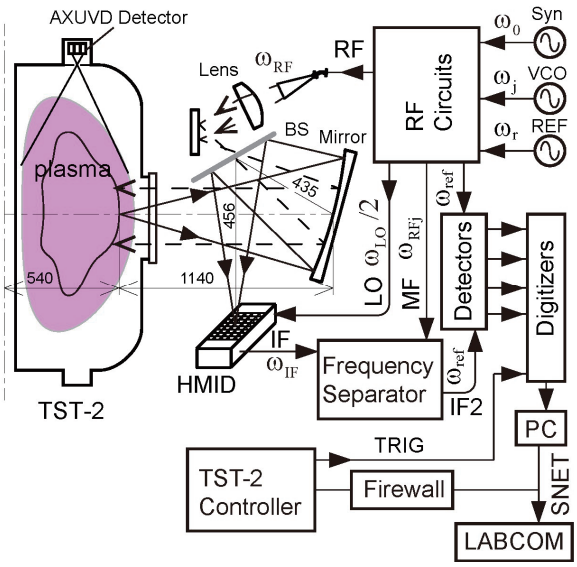


Fig. 1 Schematic diagram of the O-MIR system in TST-2.

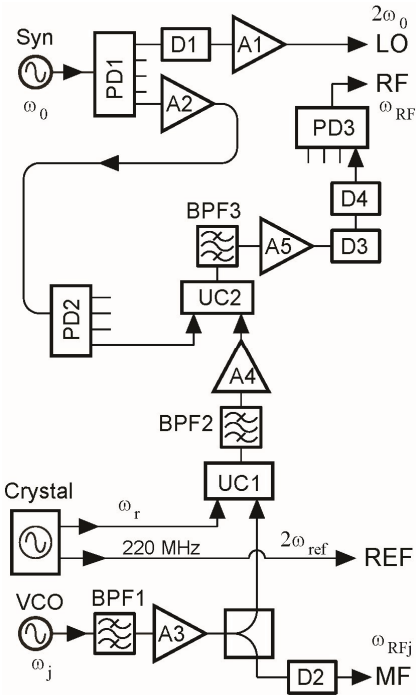


Fig. 2 Schematic diagram of the RF circuit. Syn: wave synthesizer (Phase Matrix FSL0010), VCO: voltage-controlled oscillators (mini-circuits ROS-1135-119+ and ROS-1500C-219+), Crystal: crystal oscillator (R&K OSC-221M), PD1: power divider (PD421), PD2: power divider (DMS421), D1: frequency doubler (mini-circuits ZX90-2-24-S+), D2: ×4 frequency multiplier (Wilmanco WFM-T series), D3: frequency doubler (Analog Devices HMC573LC3B), D3: frequency doubler (analog devices HMC578LC3B), A1, A2, A3, A5: RF amplifier (mini-circuits ZVA-183-AS+), A4: R&K A030), UC1, UC2 (up converters). BPF1 (1152 ± 60 MHz, 1502 ± 75 MHz), BPF2 (1152.5 ± 10 MHz, 1502 ± 10 MHz), BPF3 (6.65 ± 1.15 GHz, 7.05 ± 1.2 GHz).

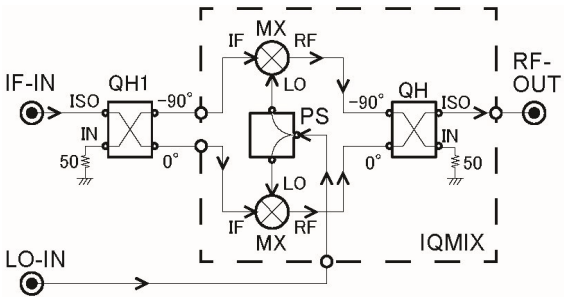


Fig. 3 Schematic diagram of up converters in Fig. 2. QH1: quadrature hybrid (R&K QH330). In UC1, MX: mixer (R&K MX170), PS: power divider (Mini-Circuits ZX10-2-12-S+). In UC2, IQMIX: I/Q mixer (analog devices HMC526LC4).

the reference wave. The detector system consists of IF amplifiers, power detectors, and IQ demodulators. The IQ demodulator produces I (= $\cos\phi$) and Q (= $\sin\phi$) signals, where $\phi$ is the phase difference between the reference wave and the detected IF wave. The detected power, I and Q signals are digitally sampled by digitizers (National Instruments PXI-6133) in PXI stations. The workstation that controls PXI stations is remotely controlled by the LABCOM system at NIFS via the virtual private network used for the Japanese fusion research named SNET [12]. The LABCOM system is linked to the TST-2 control system via a firewall between the SNET and TST-2 local area network. Digital sampling is triggered by a trigger from the TST-2 control system. The MIR data is stored and is also delivered by the LABCOM system.

The RF circuit is shown in Fig. 2. A wave synthesizer, which is controlled by a computer with a LabVIEW program, generates base frequency ($\omega_0$). Two voltage-controlled oscillators (VCO) generate additional frequencies ($\omega_j$), which are purified by band-pass filters. The reference frequency ($\omega_r$) is generated by a crystal oscillator. Using up-converters, all of those frequencies are added. The details of up-converters are shown in Fig. 3. We use two types of up-converters, as follows: UC1 for low frequency and UC2 for high frequency. UC1 consists of individual parts, and UC2 consists of a monolithic microwave integrated circuit (MMIC) and an individual part. Each up-converted RF wave is purified by a band-pass filter.

The wave synthesizer can generate a microwave up to 10 GHz, and frequencies are multiplied by ×4 frequency multipliers, $\omega_{RFj} = 4\times\omega_j$, $\omega_{ref} = 4\times\omega_r$, $\omega_{RFj}/2\pi = 4.5$ and 5.9 GHz, and $\omega_{ref}/2\pi = 110$ MHz. The actual illumination frequency ($\omega_{RF}$) is as follows: $\omega_{RF} = 4(\omega_0 + \omega_j + \omega_r) = 4\omega_0 + \omega_{RFj} + \omega_{ref}$. Finally, two waves with different frequencies are combined using a power combiner. The O-MIR system has six poloidal channels, six toroidal channels, and two radial channels. The illumination frequency can be changed between 23 GHz and 32 GHz; therefore, the observable electron density is $0.65 - 1.3\times10^{19}$ m$^{-3}$.

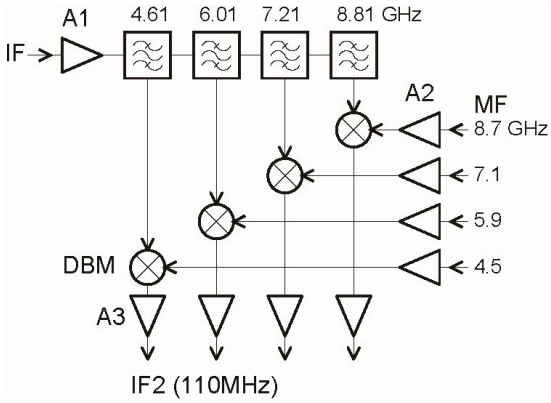


Fig. 4 Schematic diagram of the frequency separator. A1, A2, A3: RF amplifier (RFMD NBB-310), DBM: double balanced mixer (Mini-Circuits SIM-153+), BPF: micro-strip line coupler with a band pass filter.

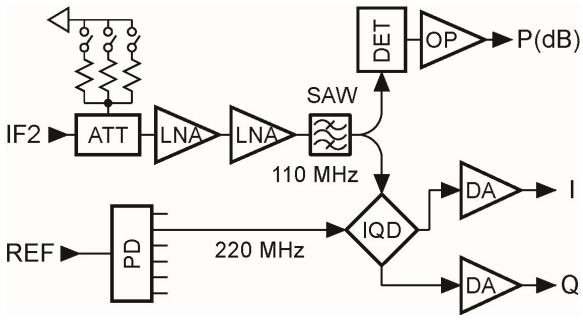


Fig. 5 Schematic diagram of the detector system. ATT: attenuator (Avago ALM38140), LNA: low noise amplifiers (Avago MGA-62563), SAW: surface-acoustic-wave filter (Murata SAFCC110MCA1T00), DET: logarithm output power detector (Analog devices AD8362), IQD: IQ demodulator (Linear Technology LT5502), OP: operational amplifier (analog devices AD8051), DA: differential amplifier (analog devices AD8130), PD: Wilkinson-type power divider.

The details of HMID are presented in ref. [10]. HMID consists of a horn-antenna array and a frequency mixer circuit on a Teflon substrate. In HMID, the signal wave ($\omega_{\rm RF}$) entering into the horn antenna is transduced to the microstrip line circuit. The local oscillation (LO) wave ($2\omega_0$) is delivered by coaxial cables to HMID, and its frequency is doubled just before entering the double balanced mixer (DBM) using an active frequency doubler. DBM mixes the RF wave ($\omega_{\rm RF}$) and LO wave ($4\omega_0$) to generate IF signals ($\omega_{\rm IF} = \omega_{\rm RF} - 4\omega_0 = \omega_{\rm RFj} + \omega_{\rm ref}$).

IF signals are separated into two frequencies using a frequency separator [5, 6], as shown in Fig. 4. Each IF signal is mixed with MF ($\omega_{\rm RFj}$) from VCO; thus all signals have the same frequency ($\omega_{\rm ref}$). The IF detection system is shown in Fig. 5. Each IF signal is amplified by MMIC amplifiers with a surface-acoustic-wave filter, which has the central frequency of $\omega_{\rm ref}/2\pi = 110$ MHz and the band width of 2 MHz. Because the IF amplifier has a very high

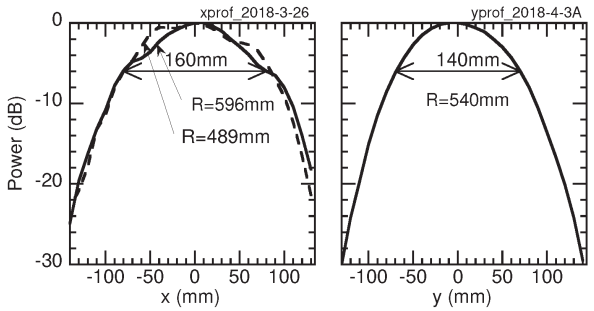


Fig. 6 Measured illumination beam profile. Horizontal and vertical distances are indicated by $x$ and $y$, respectively.

gain (> 40 dB), a semi-variable attenuator is installed at the front end. The phase is detected by a quadrature (I-Q) demodulator, for which the reference signal comes from the crystal oscillator. In this case, the frequency of the reference signal is 220 MHz owing to the requirement of an MMIC IQ demodulator. This IQ demodulator produces a differential output; thus, buffer amplifiers for I and Q signals are differential amplifiers. The power is detected by the log scale power detector. This power detector produces a single ended signal; thus, buffer amplifier is an operational amplifier.

Illumination wave is radiated by a Ka-band rectangular horn antenna and is expanded by a Teflon lens. Finally, an ellipsoidal mirror produces a parallel beam to illuminate plasma. As shown in Fig. 6, the diameter of the illumination beam is 160 mm for $R = 489$ mm and $R = 596$ mm. Here, $R$ is a radius with the major axis of the TST-2 torus. The major ($R_0$) and minor ($a_0$) radii of the TST-2 device are $R_0 = 380$ mm and $a_0 = 250$ mm, respectively. Thus, the illumination beam spot does not vary between $r/a_0 = 0.44$ and 0.86, where $r$ is the minor radius. Because IRE is supposed to take place near $R = 540$ mm, or $L_1 = 1140$ mm away from the mirror, the IRE region is illuminated by a plane wave.

Plasma reflects the illumination wave at the reflection layer of the cutoff density, which corresponds to the illumination frequency. The plasma image of the scattered wave is formed by the ellipsoidal mirror. The illumination wave and the scattered wave are coaxially mixed by a beam splitter. We tested two types of beam splitters. The first type is an acrylic plate, and the second type is a thin metal plate with many small race track-shaped holes. The later one reflects ~50% of incident beam and passes another ~50%. However, it produces a large stray wave; therefore, we use an acrylic plate.

The ellipsoidal mirror size is $400 \times 430$ mm$^2$. Thus, the effective mirror diameter is $D = 400$ mm. The measured focal length is 500 mm. The mirror is installed at $R = 1680$ mm. The scattered wave is detected by the HMID with $8 \times 8$ channels, and we use $6 \times 6$ channels. The distance between the mirror and HMID is $L_2 = 891$ mm. Thus, the detected IRE image is reduced by $L_2/L_1 = 0.78$

times. The horn size of HMID is $19.5 \times 19.5\,\mathrm{mm}^2$. The corresponding image size at the IRE area is estimated to be $25 \times 25\,\mathrm{mm}^2$.

Spatial resolution ($\delta$) can be approximately estimated by $\delta \sim (L_1/D)\lambda$, where $\lambda$ is the wavelength of the microwave. In this case the estimated resolution is $\delta \sim$ 32 mm. Figure 7 shows the power profiles of the wave scattered by a metal rod with a diameter of 40 mm on the test bench. Here, HMID channels are aligned in the toroidal direction. The channel separation and spatial resolution are 25 mm and 40 mm (full width at half maximum: FWHM), respectively. The measured channel separation is similar to the estimation, and the measured spatial resolution is worse than the estimation. Spherical aberration may deteriorate spatial resolution.

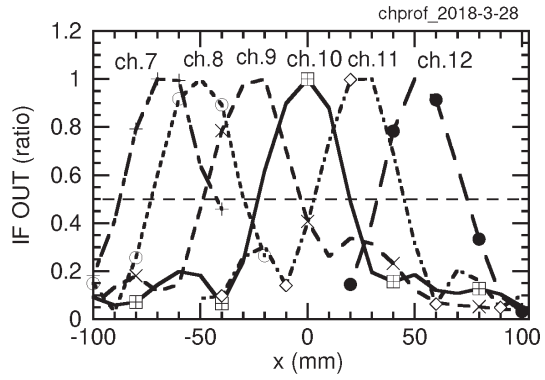


Fig. 7 Power profiles of the reflected wave by the metal rod ($\phi$40) at R = 540 mm on the test bench. The horizontal distance is indicated by $x$. Here, "ch" means the channel number of the HMID detector array.

## 3. Experiment

Figure 8 shows MIR power signals for IRE, which occurs at $t = 30\,\mu$s. At the time period T3, a pulse (red line in Fig. 8) is observed at both frequencies. The 2D images from the scattered wave power are shown in Fig. 9. Scattered power varies by more than 20 dB (100 times) both in time and space. Because the high power region is extended toroidally (in the $x$-direction), the toroidal mode number may be low. In the $y$-direction, the high power region has a narrow structure. At $t = 0\,\mu$s, it is between $y = -5$ cm and 2.5 cm; at $t = 16\,\mu$s, it is in the $y > 2$ cm region. Thus, the poloidal width of the high power region may be approximately 8 cm.

In this MIR system, two radial positions (two microwave frequencies) can be simultaneously observed. The radial structure is examined by scanning the microwave frequency shot by shot. In most shots, the pulse at IRE is observed only in the single microwave frequency. Thus, the thickness of IRE should be thin. The typical electron density profile is parabolic with the central density of

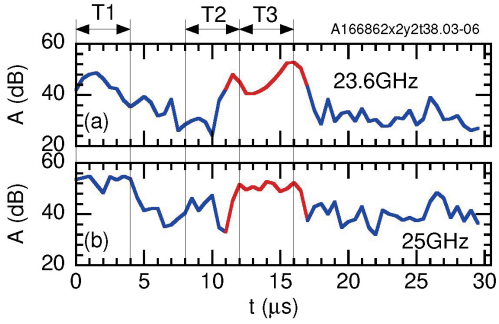


Fig. 8 Scattered microwave power. Time $t = 0$ is 13.03 ms after plasma initiation.

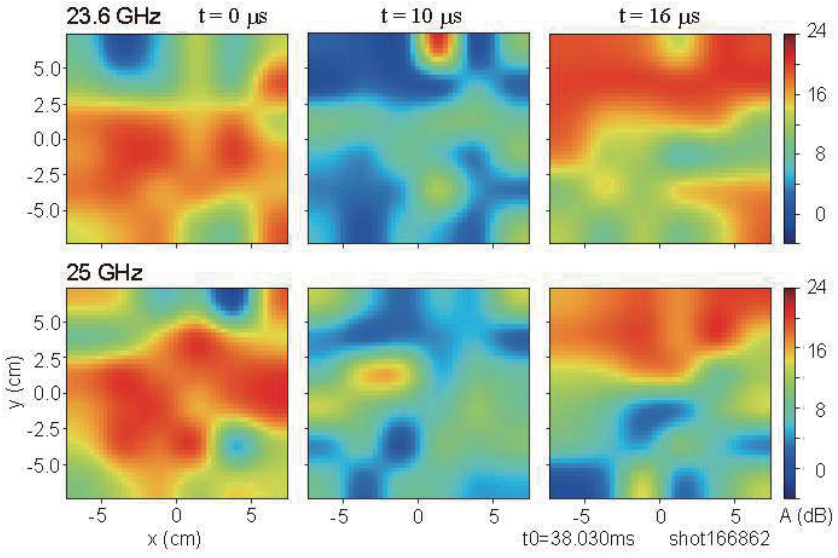


Fig. 9 2D MIR images of plasma on two reflection layers. The time period is shown in Fig. 8. Toroidal and poloidal distances are indicated by $x$ and $y$, respectively.

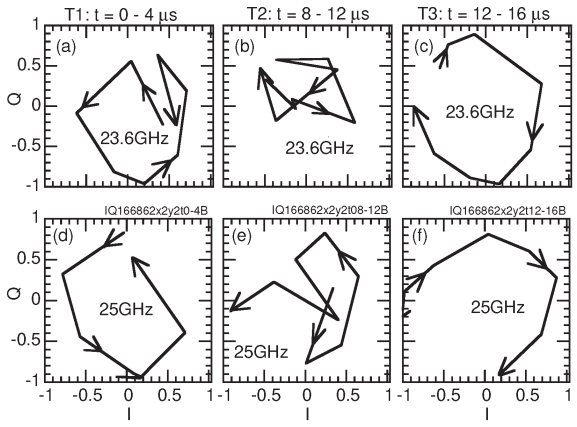


Fig. 10 Lissajous curves of I-Q signals of scattered wave. The time period is shown in Fig. 4.

$1.2 \times 10^{19}$ m$^{-3}$, which is measured by the Thomson scattering in similar plasmas. If so, illuminated microwave frequencies of 23.6 GHz and 25 GHz correspond to $r/a_0 =$ 0.65 and 0.6, respectively. Thus, two radial channels are separated by 17 mm. Therefore, the thickness of the high power region may be approximately 20 mm.

The phase change can be seen in the Lissajous curves of I-Q signals, which are shown Fig. 10. I and Q correspond to cos $\phi$ and sin $\phi$, respectively, where $\phi$ is the phase difference between the IF signal and the reference wave. At the highest power (time period T3), the I-Q Lissajous curve makes a 3/4 clockwise rotation. This indicates that the phase is decreased or the reflection surface moves outward by a 3/8 wavelength. Because the wavelength of the illuminated wave extends owing to the reduced refractive index in the plasma, the distance is more than 5 mm. In another high power period (time period T1), the I-Q Lissajous curve makes an anticlockwise rotation. Thus, plasma moves inward. When the scattered power is low (time period T2), the I-Q Lissajous curve is distorted; therefore, the phase is not determined.

A possible interpretation of the power reduction is as follows. The detected signal is an integral of the scattered wave over the detection area of each detector channel, which may be approximately $40 \times 40$ mm$^2$. If the phase of the wave varies by more than $2\pi$, the waves of different phase counteract each other to diminish the wave power. At the time period T2, the reflection surface may be tilted so that the phase of the wave in the detection area varies by more than $2\pi$.

# 4. Conclusion

The O-MIR system was installed in TST-2 to observe the IRE in ST. Of note, scattered power has quick (~5 μs) and large (> 100 times) fluctuations. A high amplitude belt structure is observed in the MIR image 20 μs before IRE. Its poloidal width is 8 cm, and its radial thickness is 2 cm. The phase measurement shows that this belt structure moves inward and outward by more than 5 mm simultaneously at $r/a \sim 0.6$. When the amplitude is low, the phase cannot be determined. It is inferred that the reduction in amplitude may be due to the phase mixing of scattered wave in each detector channel.

# Acknowledgments

This work was supported by JSPS KAKENHI Grant (17K18772), and by the NIFS Collaboration Research program (NIFS17KLEP022, NIFS17KKSP001).

[1] Y. Nagayama, K. Shinya and Y. Tanaka, IEEJ Trans. Fund. Mat. **132**, 555 (2012).
[2] H. Tojo, A. Ejiri *et al.*, Plasma Fusion Res. **2**, S1065 (2007).
[3] Z.B. Shi, Y. Nagayama, S. Yamaguchi *et al.*, Phys. Plasmas **18**, 102315 (2011).
[4] Y. Nagayama, S. Yamaguchi, Z.B. Shi *et al.*, Plasma Fusion Res. **3**, 053 (2008).
[5] S. Yamaguchi, Y. Nagayama, D. Kuwahara, T. Yoshinaga *et al.*, Rev. Sci. Instrum. **79**, 10F111 (2008).
[6] T. Yoshinaga, Y. Nagayama, D. Kuwahara *et al.*, Rev. Sci. Instrum. **81**, 10D915 (2010).
[7] Y. Nagayama, D. Kuwahara, T. Yoshinaga *et al.*, Rev. Sci. Instrum. **83**, 10E305 (2012).
[8] Y. Nagayama, S. Yamaguchi *et al.*, Plasma Fusion Res. **11**, 2402111 (2016).
[9] D. Kuwahara, N. Ito, Y. Nagayama *et al.*, Rev. Sci. Instrum. **85**, 11D805 (2014).
[10] Y. Nagayama, N. Ito, D. Kuwahara *et al.*, Rev. Sci. Instrum. **88**, 044703 (2017).
[11] Y. Takase *et al.*, Nucl. Fusion **41**, 1543 (2001).
[12] H. Nakanishi, M. Kojima, C. Takahashi, M. Ohsuna, S. Imazu *et al.*, Fusion Eng. Des. **87**, 2189 (2012).